accuracy). A similar accuracy advantage of the approximate inverse relations over the finite difference solution may exist provided that the step size in a particular problem is sufficiently large. An obvious advantage of the inverse relations is the convenience of their employment compared to the use of tables of the Prandtl-Meyer function.

References

[1]Anderson, J. D., *Modern Compressible Flow*, McGraw-Hill, New York, 1984, pp. 108–119, 263–291.

[2]Liepmann, H. W., and Roshko, A., *Elements of Gas Dynamics*, Wiley, New York, 1957, pp. 98, 99, 284–304.

[3]Özcan, O., Aslan, A. R., Edis, F. O., and Pinar, İ., "Solution of Supersonic Flow by the Method of Characteristics," *Proceedings of the 8th Congress of National Mechanics* (Antalya, Turkey), ITU Matbaasi, Istanbul, Turkey, 1993, pp. 489–498.

[4]Gerald, C. F., *Applied Numerical Analysis*, Addison-Wesley, Reading, MA, 1980, pp. 15–20.

Flow Study of Supersonic Wing-Nacelle Configuration

Kasim Biber*
Wichita State University, Wichita, Kansas 67260
and
Joel Mendoza†
NASA Ames Research Center, Moffett Field, California 94035

Introduction

NACELLE/AIRFRAME integration is of major importance for aerodynamically efficient supersonic transport aircraft design and development.[1–4] For such aircraft, nacelles are commonly positioned beneath the wing to produce relatively low wave drag. In its proper location, the nacelle should normally have an attached normal shock at its inlet lip and capture the oncoming air mass without any spillage. When the nacelle is integrated with an aircraft wing, its flowfield is affected by the wing boundary layer, depending on the nacelle proximity to the wing surface. If the nacelle inlet is placed completely outside the boundary layer, then there will be an increase of wave drag. If the wing boundary layer flows through the nacelle, then loss in total pressure and distortion in the velocity distribution will result, causing a reduction in the engine performance.[4] Therefore, the boundary layer is usually removed by means of bleed and diverter before it enters the nacelle.[3] However, such a boundary-layer control requires detailed knowledge of both isolated and integrated wing-nacelle flowfields at various Reynolds numbers, angles of attack, and wing-nacelle gaps. This article presents the results of a flow visualization study, featuring supersonic wind-tunnel tests of wing-nacelle configurations. The tests were made at Reynolds numbers, based on nacelle length, about 25 times lower than its cruise flight counterpart. Also, the nacelle exit flow would be different in flight, due to the exhaust of an operating engine. This study brings some insight into the shock-boundary-layer flow interaction between the nacelle and wing and examines the wing interference effects on the nacelle flowfield.

Received Feb. 22, 1994; revision received March 21, 1994; accepted for publication March 21, 1994.

*Postdoctoral Research Associate, National Institute for Aviation Research, Box 93. Member AIAA.

†Aerospace Engineer, Advanced Aerodynamic Concept Branch, M/S 227-6.

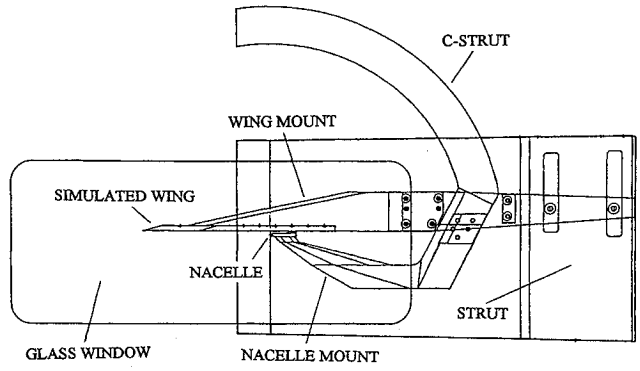

Fig. 1 Side view of the wing-nacelle model with the C-strut assembly in the tunnel test section.

Experimental Setup

The tests were conducted in a pressure-driven, intermittent, and open-circuit blowdown design supersonic wind tunnel with a 23- × 23-cm test section. The tunnel is equipped with a closed-loop servo mechanism that keeps the settling chamber pressure constant during tunnel runs.[5] The nacelle had a sharp-lip pitot intake with a 0.3-cm-diam, throughflow duct with a length-to-diameter ratio (L/D) of 9.7 and a truncated-conical exterior with 2.5-deg semivertex angle. It was mounted to the tunnel C-strut assembly through its pylon (see Fig. 1). At its zero angle of attack α setting, the nacelle was aligned with the test section centerline. The nacelle was positioned under a wing, $50D$ (diameter) streamwise distance from the wing apex. The wing simulated a delta wing, $2D$ thick, $75D$ long, and $25D$ wide flat plate planform with a 60-deg sweepback angle. When installed in the test section, the wing was parallel to the nacelle centerline, and supported separately from the nacelle so that there was no nacelle-wing strut to cause additional interference. The angles of attack were set to -2, 0, $+2$, and $+4$ deg for each wing-nacelle gaps of $0.5D$, $1D$, $2D$, and $3D$, measured from the nacelle trailing-edge location.

Test conditions were characterized by the settling chamber pressure for the flow produced by Mach 2 nozzle blocks of the tunnel. Considering the losses downstream of the nozzle throat,[6] the actual test Mach number was 1.94 ± 0.02, as determined from a shock wave angle over the flat wing, and the ratio of test section pitot pressure to settling chamber pressure. Reynolds number was calculated from the settling chamber pressure and temperature for the prescribed Mach number. The viscosity was determined from Sutherland's formula as given in Ref. 7. Tests were made for Reynolds numbers, based on nacelle length, of 1.16×10^6 and 1.45×10^6, respectively. Complete test cases are given in Ref. 8. The settling chamber pressure and, therefore, Reynolds number range, was limited by the nacelle/pylon strength. The flow unsteadiness in the settling chamber was observed qualitatively by the time history of stagnation pressures for about 10 s of tunnel runs.[5] There were fluctuations on the pressure signals, but these were below $\pm 5\%$ for the present test values.

Results and Discussion

Schlieren photographs were recorded for the flowfield of wing alone, nacelle alone, and then wing and nacelle together. Here the emphasis is given for the discussion of typical wing-nacelle results at the Reynolds number of 1.45×10^6. The nacelle had a conical oblique shock wave at its inlet lip, which remained steady and attached to the lip with α changes. The flow inside the ducted nacelle was presumably fully turbulent and free of shock waves. This is mainly because the L/D ($=9.7$) is not large enough for the internal boundary layer to create any choking flow conditions and subsequent supersonic

flow in the duct.[9] The boundary layer was turbulent in character all along the wing lower surface, as determined by comparing the visualized boundary-layer thickness with the one computed from the flat plate approximations[10] given for incompressible flow at $\alpha = 0$ deg. The boundary layer gets thinner with the increase of α, as shown in Fig. 2 for the $2D$ gap. The leading-edge shock and exhaust freejet layer at the nacelle wing-side impinge on the wing boundary layer and reflect back towards the nacelle. The shock impingement apparently does not have any effect on the already turbulent wing boundary layer. The "shock wave" reflection patterns are very similar at both $\alpha = -2$ and $+4$ deg, except that shock wave angles change with α, and as do the reflected wave angles. Furthermore, there is a slight distortion of symmetry on the nacelle exhaust flow for nonzero α, as evidenced from the location where the expansion waves cross each other.

Figure 3 shows the flow patterns for the $1D$ gap. At $\alpha = 0$ deg, the wing boundary layer is tangent to the nacelle trailing edge. The leading-edge shock impinges on the boundary layer and reflects back to the nacelle in a relatively short downstream distance. This impingement normally goes through the subsonic boundary layer until it reaches the solid surface, and its effect is felt in a region subject to an increase in the pressure. The pressure rise associated with the shock system is apparently not high enough to cause any boundary-layer separation as seen from the photographs. However, as explained in Ref. 11, there are compression waves generated by the pressure change in the subsonic layer, and these waves coalesce with the reflected wave in and out of the boundary layer. In fact, Ref. 11 also states that the turbulent boundary-layer thickness should decrease because of the interaction, but this is not evident from the present results.

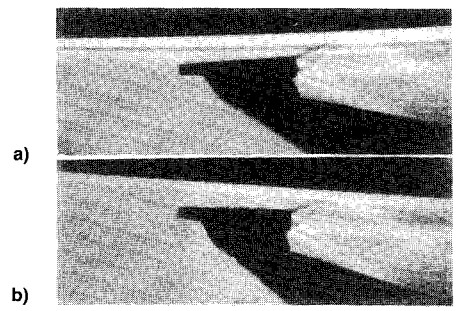

Fig. 2 Shock-boundary-layer interaction between the nacelle and wing for the gap $2D$ case at $Re_L = 1.45 \times 10^6$. α = a) -2 and b) $+4$ deg.

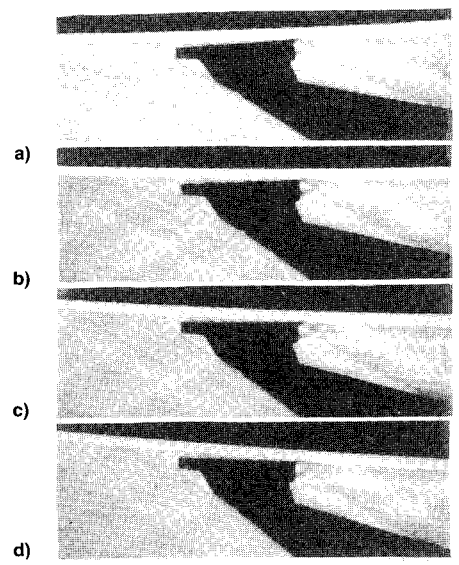

Fig. 3 Shock-boundary-layer interaction between the nacelle and wing for the gap $1D$ case at $Re_L = 1.45 \times 10^6$. α = a) -2, b) 0, c) $+2$, and d) $+4$ deg.

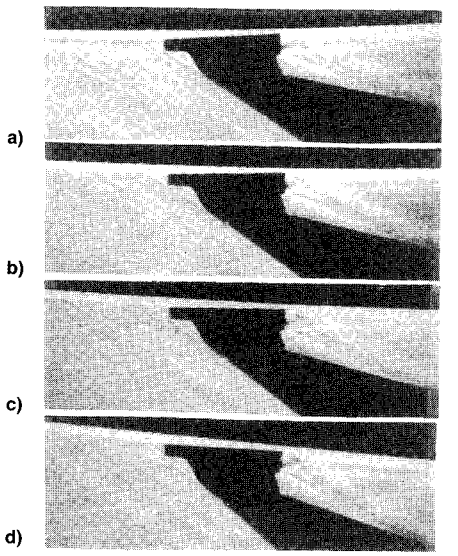

Fig. 4 Shock-boundary-layer interaction between the nacelle and wing for the gap $0.5D$ case at $Re_L = 1.45 \times 10^6$. α = a) -2, b) 0, c) $+2$, and d) $+4$ deg.

One important aspect of the present study was to bring the nacelle as close to the wing as possible and observe the interference effects. For this reason, the nacelle was positioned so that its inlet could be partially inside the wing boundary layer. As shown in the photographs (Fig. 4), the nacelle leading-edge shock wave at the wing-side is completely absent, and there is an attached shock wave from the nacelle lower (windward for $\alpha \geq 0$ deg) side. The wing boundary layer appears to have no effect on the inlet normal shock. For the thickest boundary layer (at $\alpha = -2$ deg), a small fraction of the wing boundary layer is entering the nacelle. As it travels inside the nacelle duct, it evidently thickens the internal boundary layer and partially distorts the internal velocity distribution. How much thickness the wing boundary layer adds to the duct is not seen in the photographs, but its effect on the flowfield becomes more pronounced at the nacelle exit. The wing boundary layer just after the nacelle shows an increased thickness, and it prevents the formation of one of the branches of the exit expansion waves. The increase of thickness is also a result of the additional turbulence produced by the nacelle entry to the wing boundary layer. As α is increased from -2 to $+4$ deg, there is a decrease in the wing boundary layer entering the duct and, hence, in the boundary-layer thickness just downstream from the nacelle. Furthermore, the nacelle exhaust flow appears to show a lessened effect of the wing boundary-layer impingement. For this test case, the nacelle exit flow discharges into the wing boundary-layer flow. Since the boundary layer has lower velocity than both the freestream and the nacelle exit flow, an overexpansion wave pattern occurs for the region where the nacelle exit is inside the wing boundary layer. The occurrence of both under- and overexpansion flow for the same nacelle exit flow creates a rather complex phenomenon, and is not clearly defined in the photographs. The merits of designing nacelles that do not ingest boundary-layer flow are evident from these photographs.

Conclusions

1) The nacelle leading-edge shock wave appears to be steady and attached to the inlet lip for all test cases.

2) The boundary layer on the wing lower surface is turbulent and the shock-expansion waves from the nacelle do not have a significant impingement effect on its character.

3) The wing boundary-layer thickness is equal to the wing-nacelle gap of $1D$ at the nacelle trailing edge when $\alpha = 0$ deg.

4) For the smallest gap, $0.5D$, the nacelle inlet is partially inside the wing boundary layer. At $\alpha = -2$ deg, some boundary layer enters the nacelle and distorts the nacelle exhaust flow symmetry. The amount of wing boundary layer flowing through the nacelle and the associated distortion are lessened with the increase of α.

Acknowledgment

This work was supported by NASA Ames Research Center under Contract A24888D(MXR).

References

[1]Rech, J., and Leyman, C. S., "Concorde Aerodynamics and Associated Systems Development," *A Case Study by Aerospatiale and British Aerospace on the Concorde*, AIAA Professional Study Series, Sec. 6, 1980, pp. 1–39.

[2]Carter, E. C., "Experimental Determination of Inlet Characteristics and Inlet and Airframe Interference," *Airframe/Engine Integration*, edited by A. Ferri, AGARD Lecture Series 53, Paper 3, May 1972, pp. 1–23.

[3]Leynaert, J., Surber, L. E., and Goldsmith, E. L., "Transport Aircraft Intake Design," *Practical Intake Aerodynamic Design*, edited by E. L. Goldsmith and J. Seddon, AIAA Education Series, AIAA, Washington, DC, 1993, pp. 218–231.

[4]Kuchemann, D., *The Aerodynamic Design of Aircraft*, Pergamon, Oxford, England, UK, 1978, pp. 56–102.

[5]Biber, K., "Calibration and Use of WSU 9 × 9-inch Supersonic Wind Tunnel," Wichita State Univ., NIAR Rept. 93-17, Wichita, KS, July 1993.

[6]Pope, A., and Goin, L. K., *High-Speed Wind Tunnel Testing*, Krieger, Malabar, FL, 1965, pp. 50–53.

[7]NASA Ames Research Staff, "Equations, Tables, and Charts for Compressible Flow," NACA Rept. 1135, 1953.

[8]Biber, K., and Ellis, D. R., "Supersonic Flow Visualization of a Nacelle in Close Proximity to a Simulated Wing," Wichita State Univ., NIAR Rept. 93-18, Wichita, KS, July 1993; also see AIAA Paper 94-0670, Jan. 1994.

[9]Shapiro, A. H., *The Dynamics and Thermodynamics of Compressible Fluid Flow*, Vol. I, Wiley, New York, 1953, pp. 170–173.

[10]Schlichting, H., *Boundary-Layer Theory*, 7th ed., McGraw-Hill, New York, 1979, pp. 24–46.

[11]Green, J. E., "Interactions Between Shock Waves and Turbulent Boundary Layers," *Progress in Aerospace Sciences*, Vol. 11, edited by D. Kuchemann, Pergamon, Oxford, England, UK, 1970, pp. 235–340.

Analytic Prediction of Lift for Delta Wings with Partial Leading-Edge Thrust

Lance W. Traub*
University of the Witwatersrand, Johannesburg, South Africa

Nomenclature

AR = aspect ratio, b^2/S
b = wing span
C_D = drag coefficient
C_{Di} = lift dependent drag coefficient
C_{Do} = zero lift drag coefficient
C_L = lift coefficient
C_N = attached flow normal force coefficient
C_{SE} = side-edge suction coefficient
C_T = theoretical wing thrust coefficient
$C_{T_{eff}}$ = overall leading-edge thrust coefficient
c = local wing chord
c_R = wing root chord
c_t = sectional theoretical thrust coefficient
k_i = induced drag constant
k_p = potential constant
r = leading-edge radius
S = wing area
α = angle of attack
η = nondimensional spanwise coordinate, $2y/b$
η_s = spanwise position at which the leading-edge drag equals the leading-edge thrust
η_T = spanwise position at which attainable thrust is equal to theoretical thrust
Λ_{LE} = leading-edge sweep angle
λ = taper ratio

Received Nov. 15, 1992; revision received July 19, 1993; accepted for publication Aug. 2, 1993.

*Graduate Student, School of Mechanical Engineering, Branch of Aeronautical Engineering, 1 Jan Smuts Ave., P.O. Wits, 2050.

Introduction

HIGH subsonic and supersonic flight has necessitated the use of thin slender wings to reduce drag. These wings are typically characterized by flow separation at low angles of attack. For slender wings the separated flow leads to the formation of leading-edge vortices which, in turn, give rise to additional nonlinear vortex lift. Polhamus[1,2] successfully accounted for this additional lift by means of a leading-edge suction analogy (where the leading-edge suction force is assumed to rotate through 90 deg and supplement the normal force coefficient). Bradley et al.[3] extended the analogy to include wings with curved leading edges. The theory of Polhamus predicts the overall force coefficients, but gives no indication of spanwise distributions. Purvis[4] derived analytic equations based on Polhamus' analogy to predict the characteristics of sharp-edged generalized planforms by determining an expression for their leading-edge thrust distribution. Some computational techniques that model slender wings use the suction analogy and model the lifting surface using a vortex lattice,[3] whereas others model the wake using discrete load-free filaments.[5] Although the suction analogy is successful, the influence of the aerofoil geometry and its effects on the amount of leading-edge thrust developed (or the attainable thrust) is not accounted for. It is assumed that the leading edge is sharp and that flow separation is total, so that no leading-edge thrust is developed.

Carlson and Mack[6] determined empirical relations to relate the attainable leading-edge thrust to various aerofoil geometric parameters, as well as Reynolds and Mach number. Kulfan[7,8] surmised that local leading-edge separation occurs when a profile's leading-edge thrust is equal to its leading-edge drag (giving rise to a separation bubble or, on slender wings, the development of vortex lift). Reference 9 gives an expression for the leading-edge drag, which enables the determination of the incidence at which separation occurs, as well as allowing estimation of the attainable thrust, and on slender wings—the vortex lift. To utilize either of these approaches a theoretical distribution of leading-edge thrust is required. This is usually determined by computational methods. It is, however, desirable for the purposes of preliminary design, to have simple analytic expressions for estimates of lift and drag of slender planar delta wings where the leading edges are not necessarily sharp, and where nonlinear effects can be accounted for.

Incompressible expressions for lift and drag are derived for basic and cropped delta wings. Separate expressions are determined based on the empirical relations of Ref. 6, and the method of Kulfan.[7,8] The expressions are evaluated and compared with experimental results.